Monthly Notices of the ROYAL ASTRONOMICAL SOCIETY

MNRAS **508,** 1526–1532 (2021) https://doi.org/10.1093/mnras/stab2619
Advance Access publication 2021 September 15

Modelling the insertion of O(^{1}D) into methane on the surface of interstellar ice mantles

Joshua T. Carder [1]★ Wyatt Ochs[2] and Eric Herbst[1,3]

[1]*Department of Chemistry, University of Virginia, McCormick Road, Charlottesville, VA 22904, USA*
[2]*College of Chemistry, University of California, Berkeley, 420 Latimer Hall, Berkeley, CA 94720, USA*
[3]*Department of Astronomy, University of Virginia, McCormick Road, Charlottesville, VA 22904, USA*

Accepted 2021 September 2. Received 2021 August 27; in original form 2021 July 6

ABSTRACT

The detection of many complex organic molecules (COMs) in interstellar space has sparked the study of their origins. While the formation of COMs detected in hot cores is attributed to photochemistry on warming grain surfaces followed by recombination of radicals and desorption, the formation routes in colder regions are still a debated issue with a number of theories such as cosmic ray bombardment on interstellar ice mantles or non-diffusive surface chemistry. Here, we present another method with reactions involving metastable atomic oxygen in the O(^{1}D) state, which is initially produced by photodissociation of oxygen-containing species in interstellar ices. As a first example, we study the reactions of metastable oxygen atoms and methane in ices to form both formaldehyde and methanol. The reaction is studied incorporating two different surface processes: diffusive and non-diffusive chemistry. The formation of methanol and formaldehyde via metastable oxygen atoms is compared with well-known formation routes of both to understand the O(^{1}D) contributions at different temperatures.

Key words: astrochemistry – ISM: molecules.

1 INTRODUCTION

Observations of complex organic molecules (COMs) are ubiquitous throughout different stages of star formation from molecular clouds to protoplanetary discs (e.g. Blake et al. 1987; Öberg et al. 2010). Such findings warrant a large number of studies concerning the formation mechanisms of these molecules in interstellar environments. The formation of COMs has typically been modelled mainly by diffusion and recombination of large radicals on the surface of interstellar grains during the warm-up phase of cloud collapse to form hot cores (Garrod, Widicus Weaver & Herbst 2008). Observations of cold sources, however, reveal the presence of COMs predating the warm-up phase such as the recent detections of unsaturated molecules and oxygen-bearing COMs in the Taurus Molecular Cloud (e.g. Agúndez et al. 2021; Lee et al. 2021). Therefore, a cold mechanism must be present that can efficiently produce COMs at the low temperatures of dark clouds.

One of the most efficient low-temperature reaction paths is the hydrogenation of species on grain surfaces due to the relatively low diffusion barrier of atomic hydrogen. This mechanism has been shown to be efficient in forming methanol and formaldehyde (Watanabe & Kouchi 2002; Fuchs et al. 2009):

$$\mathrm{CO} \xrightarrow{\mathrm{H}} \mathrm{HCO} \xrightarrow{\mathrm{H}} \mathrm{H_2CO} \xrightarrow{\mathrm{H}} \mathrm{CH_3O/CH_2OH} \xrightarrow{\mathrm{H}} \mathrm{CH_3OH}, \quad (1)$$

as well as in the formation of terminally saturated products such as methane, which has been shown to be efficient in both carbon monoxide (Hiraoka et al. 1998) and water ice (Qasim et al. 2020):

$$\mathrm{C} \xrightarrow{\mathrm{H}} \mathrm{CH} \xrightarrow{\mathrm{H}} \mathrm{CH_2} \xrightarrow{\mathrm{H}} \mathrm{CH_3} \xrightarrow{\mathrm{H}} \mathrm{CH_4}. \quad (2)$$

Such hydrogen additions are found to be most efficient at low temperatures (<15 K) before the thermal desorption of atomic hydrogen becomes competitive with its diffusion (Fuchs et al. 2009). Additionally, these routes only involve partially saturated species in order to form the fully saturated closed-shell counterpart. This limits the production of COMs to the hydrogenation of heavy atoms such as oxygen, nitrogen, etc. into grain species. The inclusion of excited metastable species, if sufficiently long-lived, could produce other compounds by reacting with abundant closed-shell molecules on or within ices and thereby stimulating COM production.

These metastable species are formed via energetic processing by either radiolysis or photodissociation. Radiolysis, caused by cosmic ray bombardment of carbon-containing ice mantles, and known as irradiation, can lead to the presence of electronically and vibrationally excited neutral radical species that eventually enhance COM formation in cold regions of molecular clouds. Radiolysis has been invoked in astrochemical models by Shingledecker et al. (2018). Photodissociation is typically modelled under the assumption that any fragments are produced in the electronically ground state and go on to recombine with other radicals. On the other hand, the synthetic power of metastable atomic species produced by photodissociation such as the first excited state of atomic oxygen, O(^{1}D), is a relatively unexplored topic in astrochemical models. Once formed, O(^{1}D) provides a method for barrierless reactions with interstellar species while providing a source of oxygen in COM production.

The metastable oxygen atom has been shown to react with gas phase species such as methane where vibrationally excited methanol

★ E-mail: jtc3wv@virginia.edu

© 2021 The Author(s)
Published by Oxford University Press on behalf of Royal Astronomical Society

Downloaded from https://academic.oup.com/mnras/article/508/1/1526/6370606 by University of Virginia Law Library user on 06 July 2022

is formed and dissociates into fragments:

$$CH_4 + O(^1D) \rightarrow CH_3OH^* \rightarrow CH_3 + OH, \quad (3)$$

unless collisionally de-excited by a third body in dense conditions which are highly unlikely in molecular clouds (DeMore & Raper 1967). Additionally, the lifetime of O(¹D), 116s (Wiese, Smith & Miles 1966), is far too short to collisionally react in the gas phase before phosphorescence to the ground O(³P) state, which eliminates the possibility of reactivity involving the excited state. Therefore, any gas phase contribution of O(¹D) to the formation of methanol or other products would only be feasible in dense environments not typically found in the interstellar medium.

The surface of interstellar ice mantles provides a more likely medium for reactions, especially insertion reactions, which refer to the inclusion of a species into an existing bond before de-excitation, where any excited product can be stabilized by the grain. Bergner, Öberg & Rajappan (2017) showed experimentally that O(¹D) reacts efficiently at low temperatures (9–25 K) on ice surfaces. After co-depositing methane and molecular oxygen, the authors observed the formation of both methanol and formaldehyde upon irradiation by ultraviolet (UV) light with respective branching ratios of approximately 0.65 and 0.35 without any observable temperature dependence. With direct detection of methanol and formaldehyde during irradiation, the production was attributed to a metastable oxygen insertion:

$$CH_4 + O(^1D) \rightarrow CH_3OH^* \rightsquigarrow CH_3OH \quad (4)$$

$$CH_4 + O(^1D) \rightarrow CH_3OH^* \rightsquigarrow H_2CO + H_2, \quad (5)$$

where the initially formed excited methanol is stabilized by the surface to form closed-shell products methanol and formaldehyde rather than the dissociative channel of reaction (3) observed in the gas phase. Because of the lack of an observed energy barrier, this mechanism holds the potential of being an important methanol production route in cold sources and in warmer environments where hydrogen addition is less efficient given the rapid thermal desorption of hydrogen atoms.

For the above mechanism to be effective, a supply of metastable excited oxygen atoms is needed. The ice surface on interstellar grains is known to contain oxygen-bearing molecules that produce O(¹D) upon photodissociation such as H_2O and CO_2 (Gibb et al. 2004). Water is of particular interest because it is the most abundant molecule in interstellar ice mantles and photodissociates into H_2 and O(¹D) with an efficiency of 10 per cent (Slanger & Black 1982). Carbon dioxide also photodissociates to form O(¹D) but with an efficiency closer to unity, and due to its high abundance of up to 30 per cent that of water (Öberg et al. 2011), it has the potential of being a large contributor of excited oxygen atoms (Schmidt, Johnson & Schinke 2013). Though molecular oxygen is difficult to detect directly in interstellar ices, it has been observed to be a relatively large component of the comet 67P/Churyumov–Gerasimenko with formation suspected to predate the creation of the comet (Bieler et al. 2015). Some models have shown that the abundance of O_2 can be attributed at least in part to formation during the dark cloud stage (Taquet et al. 2016) making this molecule a viable producer of O(¹D) in ice mantles and similarly ozone due to its abundance being tied to O_2 via:

$$O_2 + O \rightarrow O_3. \quad (6)$$

Furthermore, both molecular oxygen and ozone form O(¹D) with efficiencies of about unity when irradiated by high-energy UV photons (Ndengué et al. 2014; Heays, Bosman & van Dishoeck 2017).

After O(¹D) is photoproduced, the atom has three outcomes: diffusion, de-excitation, or reaction. Diffusion being a thermal process is rather slow at low temperatures, and de-excitation will occur more rapidly either radiatively or collisionally where lifetimes have been observed to be of the order of 1s in matrices (Mohammed 1990). Reaction is the most likely outcome due to the high reactivity of O(¹D) and the presence of adjacent reaction partners. Although a number of mechanisms involving adjacent partners were formulated by Jin & Garrod (2020), the greatest interest here is the mechanism where photodissociation produces O(¹D) which then reacts with an adjacent neighbour, a mechanism termed photodissociation-induced reactions (PDI). This process was first studied in cometary ices by Garrod (2019) and used further in molecular cloud models by Jin & Garrod (2020). Such reaction mechanisms are further coupled with reactive desorption where the excess exothermicity of the reaction can liberate a fraction of any formed products from the surface and into the gas phase (Garrod, Wakelam & Herbst 2007).

In this work, we report our study of the contribution of the oxygen insertion of O(¹D) into methane to form methanol and formaldehyde on the surface of granular ice mantles. Additional insertion reactions involving O(¹D) will be included for multiple adjacent reaction partners while using the PDI mechanism proposed by Garrod (2019) to understand its effect on formaldehyde and methanol abundances in cold cores. Section 2 contains an overview of the model utilized while Section 3 presents our results. Section 4 contains any implications this new production mechanism could have in interstellar molecular clouds. Finally, Section 5 contains our conclusions.

2 MODEL

The simulations conducted in this work utilized the three-phase gas–grain code `Nautilus-1.1` (Ruaud, Wakelam & Hersant 2016) where the three phases are represented by the gas and the surface and bulk mantle of the ice. The surface is assumed to encompass the top two monolayers of the ice where the bulk is the remainder. As defined in the introduction, PDIs were added to the code to include the mechanisms used by Garrod (2019) and Jin & Garrod (2020) where photodissociation can be caused by UV radiation from the interstellar UV field and, at sufficient visual extinction, the secondary UV field produced by cosmic rays. Additionally, a diffusive mechanism where the excited oxygen can hop or tunnel over diffusive barriers and react in different grain sites was implemented as a check if diffusion is a significant contributor to O(¹D) insertion reactions. The formulation will be discussed further below. For any reactions occurring between surface species, a reactive desorption efficiency was assumed to occur with an efficiency of 1 per cent (Garrod et al. 2007). All initial elemental abundances are given in Table 1, and physical conditions are shown in Table 2 where N_{site} is the site density on the surface of the grains, ζ is the cosmic ray ionization rate of H_2, and A_v is the visual extinction. The temperatures of both the gas and the grain were assumed to be the same and were varied for different models from 10 to 20 K.

The reaction network was expanded to include both photoproduction pathways and reactions involving O(¹D). All photoproductive rates to produce O(¹D) were taken from equivalent gas phase rates from the KIDA network (Wakelam et al. 2012) and were assumed to produce the excited state of oxygen rather than the ground state. This assumption is valid due to spin conservation as long as the reactant is in a singlet state or has the same spin as the non-oxygen product. These productive routes and equivalent rates are given in Table 3. The

Downloaded from https://academic.oup.com/mnras/article/508/1/1526/6370606 by University of Virginia Law Library user on 06 July 2022

Table 1. Initial elemental abundances utilized in the models.

Species	Abundance
H_2 [a]	0.499
He[a]	9.000×10^{-2}
C[b]	1.700×10^{-4}
N[a]	6.200×10^{-5}
O[c]	2.429×10^{-4}
F[e]	6.680×10^{-9}
S[d]	8.000×10^{-8}
P[d]	2.000×10^{-10}
Cl[d]	1.000×10^{-9}
Na[d]	2.000×10^{-9}
Mg[d]	7.000×10^{-9}
Fe[d]	3.000×10^{-9}

[a]Wakelam & Herbst (2008)
[b]Jenkins (2009)
[c]McGuire et al. (2018)
[d]Graedel, Langer & Frerking (1982)
[e]Neufeld, Wolfire & Schilke (2005)

Table 2. Physical conditions used to model dark clouds.

Parameter	Value
n_H (cm^{-3})	10^4
n_{dust} (cm^{-3})	1.8×10^{-8}
N_{site} (cm^{-2})	1.5×10^{15}
ζ (s^{-1})	1.3×10^{-17}
A_v	10

Table 3. The reactions and associated rates from the KIDA network (Wakelam et al. 2012) utilized in the models for forming $O(^1D)$.

Reaction	Rate coefficient [s^{-1}]
$CO_2 \xrightarrow{UV} CO + O(^1D)$	$3.13 \times 10^{-10}\exp(-2.03A_V)$
$H_2O \xrightarrow{UV} H_2 + O(^1D)$	$1.90 \times 10^{-10}\exp(-3.10A_V)$
$O_2 \xrightarrow{UV} O(^3P) + O(^1D)$	$3.30 \times 10^{-10}\exp(-1.40A_V)$
$O_3 \xrightarrow{UV} O_2 + O(^1D)$	$1.00 \times 10^{-9}\exp(-1.70A_V)$
$ClO \xrightarrow{UV} Cl + O(^1D)$	$1.00 \times 10^{-10}\exp(-2.00A_V)$
$N_2O \xrightarrow{UV} N_2 + O(^1D)$	$1.40 \times 10^{-9}\exp(-1.70A_V)$
$CO_2 \xrightarrow{CRUV} CO + O(^1D)$	$1.71 \times 10^{+3}\zeta$
$O_2 \xrightarrow{CRUV} O(^3P) + O(^1D)$	$7.50 \times 10^{+2}\zeta$
$O_3 \xrightarrow{CRUV} O_2 + O(^1D)$	$1.50 \times 10^{+3}\zeta$
$ClO \xrightarrow{CRUV} Cl + O(^1D)$	$5.00 \times 10^{+2}\zeta$

insertion reactions into methane were added including the branching ratios given by Bergner et al. (2017). Additional reactions with $O(^1D)$ were added in order to simulate competition of the excited oxygen reacting with other grain species with product channels and branching ratios based on gas phase reactions due to lack of experimental surface and computational studies. Therefore, the product routes used are likely unrealistic as they prefer dissociation into fragments rather than the closed-shell products seen by reactions (4) and (5). All added reactions with respective branching ratios are given in Table 4.

The formalism we use for PDIs was first discussed by Garrod (2019) and used specifically for reactions involving $O(^1D)$. The reaction scheme starts with

$$A \xrightarrow{h\nu} B + C^*, \tag{7}$$

Table 4. The reactions of $O(^1D)$ and additional species added to the models with associated branching ratios (BR).

Reaction	BR	Reference
$O(^1D) + CH_4 \rightarrow CH_3OH$	0.65	Bergner et al. (2017)
$O(^1D) + CH_4 \rightarrow H_2CO + H_2$	0.35	Bergner et al. (2017)
$O(^1D) + H_2O \rightarrow 2OH$	0.90	Dunlea & Ravishankara (2004b)
$O(^1D) + H_2O \rightarrow H_2O + O(^3P)$	0.10	Takahashi et al. (1996)
$O(^1D) + CO \rightarrow CO + O(^3P)$	0.90	Raper & DeMore (1964)
$O(^1D) + CO \rightarrow CO_2$	0.10	Raper & DeMore (1964)
$O(^1D) + H_2 \rightarrow OH + H$	1.00	Talukdar & Ravishankara (1996)
$O(^1D) + NH_3 \rightarrow OH + NH_2$	1.00	Davidson et al. (1977)
$O(^1D) + HF \rightarrow OH + F$	1.00	Atkinson et al. (2007)
$O(^1D) + NO_2 \rightarrow O_2 + NO$	1.00	Heidner & Husain (1973)
$O(^1D) + N_2O \rightarrow N_2 + O_2$	0.60	Lam et al. (1981)
$O(^1D) + N_2O \rightarrow 2NO$	0.40	Lam et al. (1981)
$O(^1D) + O_3 \rightarrow 2O_2$	0.50	Dunlea & Ravishankara (2004a)
$O(^1D) + O_3 \rightarrow O_2 + 2O(^3P)$	0.50	Dunlea & Ravishankara (2004a)
$O(^1D) + HCl \rightarrow OH + Cl$	0.80	Chichinin (2000)
$O(^1D) + HCl \rightarrow H + ClO$	0.20	Chichinin (2000)

which is followed by

$$C^* + D \rightarrow \text{Products} \tag{8}$$

with an asterisk denoting an electronically excited species. The first reaction involves the photodissociation of species A to form fragments B and electronically excited C^* while our model is only concerned with $O(^1D)$ production. Photodissociation is followed by the reaction of C^* with an adjacent partner D to form the final set of products. In the case of $O(^1D)$, reaction (8) typically proceeds barrierlessly making the process virtually instantaneous following the cleavage of A, so that reactions (7) and (8) effectively form a single reaction step involving A and D to produce the product. Therefore, the final rate of the reaction (s^{-1}) is the rate of reaction (7) multiplied by the probability that D is an adjacent reactive partner:

$$R = R_{\text{Photolysis}}(\text{A})\frac{N(\text{D})}{N_{\text{S/M}}}, \tag{9}$$

where $N(i)$ represents the number of species i on the surface or in the bulk, and $N_{S/M}$ is similarly the number of sites on the surface (S) or in the bulk (M). PDIs involving both surface and bulk species were included in the models.

The value of $R_{\text{Photolysis}}$ (s^{-1}) depends upon the mechanism of photodissociation from the external UV field, shown in equation (10), or the cosmic ray induced secondary UV field generated from the Prasad–Tarafdar mechanism (Prasad & Tarafdar 1983), shown in equation (11):

$$R_{\text{UV}}(i) = k\exp(-CA_v)N(i) \tag{10}$$

$$R_{\text{CRUV}}(i) = \alpha\zeta N(i). \tag{11}$$

Here, k represents the unattenuated photodissociation rate coefficient (s^{-1}) of the reactant in the Draine field (Draine 1978), and the term $\exp(-CA_v)$ attenuates the rate coefficient due to the shielding of dust particles at a particular visual extinction, A_v. The value of C depends in part upon the photodissociation threshold of the reactant in question. The rate for cosmic ray induced photodissociation of species i, shown in equation (11), consists of the product of ζ, the cosmic ray ionization rate of H_2, and α the factor unique for each species. The form taken by α is discussed further by Wakelam et al. (2012). Both types of photodissociation rates were assumed to have the same efficiency as their gas phase counterparts.

Downloaded from https://academic.oup.com/mnras/article/508/1/1526/6370606 by University of Virginia Law Library user on 06 July 2022

The diffusive mechanism for O(¹D) reactions follows the same reaction scheme shown in reactions (7) and (8) with photoproduction of O(¹D) occurring first and diffusion on the grain surface required for the reaction to occur. The photoproduction step of reaction (7) follows the same rate as equations (9) and (10) depending on the source of the UV field while reaction (8) follows the diffusion rate at surface temperature T:

$$R = \nu(\mathrm{C^*})\exp\left(-\frac{E_{\mathrm{diff}}(\mathrm{C^*})}{T}\right)\frac{N(\mathrm{D})}{N_{\mathrm{S/M}}} + \nu(\mathrm{D})\exp\left(-\frac{E_{\mathrm{diff}}(\mathrm{D})}{T}\right) \times \frac{N(\mathrm{C^*})}{N_{\mathrm{S/M}}}, \quad (12)$$

where ν and E_{diff} are the characteristic vibrational frequency and diffusion barrier of the species, respectively, with the vibrational frequency calculated under a harmonic approximation (Hasegawa, Herbst & Leung 1992). The diffusion barrier of O(¹D) was assumed to be the same as its ground state counterpart (1600 K) (Wakelam et al. 2017). Due to the instability of the singlet state, any diffusion will not be competitive with either radiative decay or reaction with an adjacent species on the grain. Therefore, this approximation is used simply for a diffusive test case where in actuality the barrier would differ from the triplet state. The radiative relaxation was treated via exponential decay with a measured radiative lifetime of 1s (Mohammed 1990) as found for matrices. This value was used only for the diffusive mechanism since the metastable oxygen reacts immediately upon formation when invoking the non-diffusive mechanism.

3 RESULTS

To study the contribution of O(¹D) insertion into methane, three different models were utilized. Model 1, our base model, has no photolysis routes to produce O(¹D) and no follow-up reactions involving O(¹D) added to the reaction network. This model contains the production of methanol and formaldehyde produced by the usual method of surface hydrogenation of CO as contained in the gas–grain Nautilus network. Model 2 has the same network as the base model except for the inclusion of O(¹D) formation reactions, shown in Table 3, and O(¹D) surface reactions as shown separately in Table 4, occurring via the standard diffusive mechanism formulated by equation (12). Finally, Model 3 starts with the same chemistry as Model 2 but also contains O(¹D) instantaneous surface reactions following photolysis as shown in equations (9) via process (10) or (11) depending on the source of radiation. The fractional abundances with respect to hydrogen nuclei of formaldehyde and methanol from the models are shown as functions of time in Figs 1, 2, and 3 for grain and gas temperatures of 10, 15, and 20 K, respectively. Each model is represented by either a solid line (Model 1), a dotted line (Model 2), or a dashed line (Model 3). Fig. 4 presents a ratio between the abundances of Model 2 to Model 1 shown by dotted lines and Model 3 to Model 1 shown by dashed lines where the left-hand panels contain methanol abundance ratios and right-hand panels formaldehyde abundance ratios. The top, middle, and bottom panels signify models that were run at 10, 15, and 20 K, respectively. All figures include data for all three phases modelled: gas (red), surface (blue), and mantle (green).

As can be seen in Fig. 1, any difference between Model 1 and Model 2 is not visible. This lack of distinction results from the large diffusive barrier, which is too high to allow significant movement and subsequent reaction before O(¹D) undergoes phosphorescence back down to the ground state. Moreover, it is unrealistic for the excited oxygen to prefer diffusion over a thermal barrier when it can react

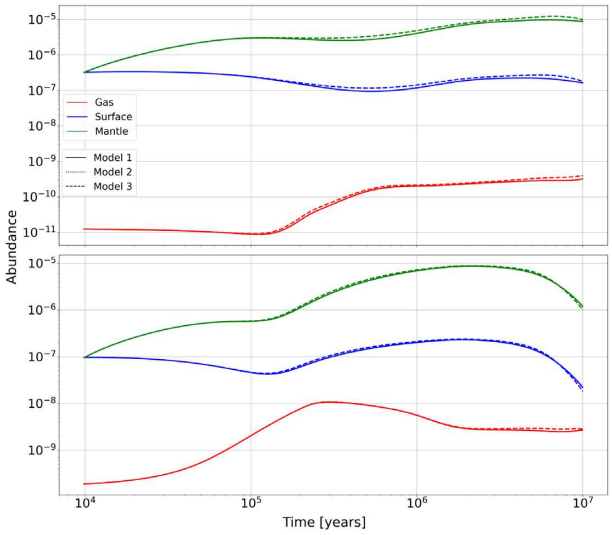

Figure 1. The abundances with respect to hydrogen nuclei of methanol (top panel) and formaldehyde (bottom panel) in Model 1, Model 2, and Model 3 at 10 K.

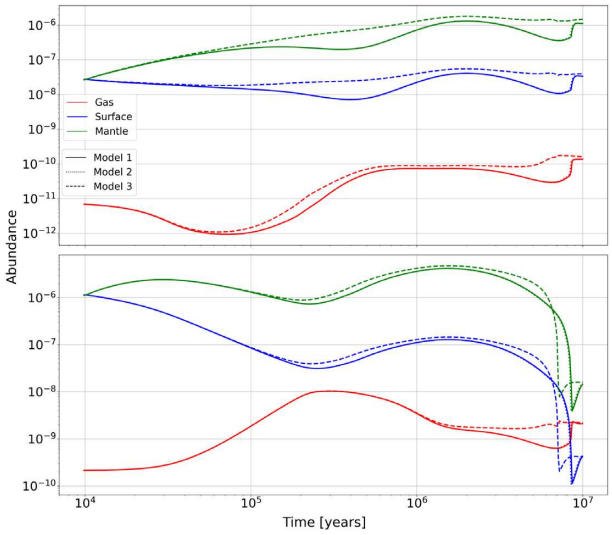

Figure 2. The abundances with respect to hydrogen nuclei of methanol (top panel) and formaldehyde (bottom panel) in Model 1, Model 2, and Model 3 at 15 K.

barrierlessly with its nearest neighbours on the grain. At the other two temperatures, 15 and 20 K, in Figs 2 and 3, respectively, similar behaviour is exhibited with no increase in the distinction between Models 1 and 2. The only slight increase is shown by Fig. 3 at times later than 10^6 yr indicating that the diffusive mechanism becomes faster with increasing temperatures. However, this test case overall shows that diffusion is far too limited by the cold cloud conditions to contribute sufficiently to formaldehyde and methanol production via O(¹D) reactions.

At first glance, the abundances of formaldehyde and methanol with Model 3 at 10 K are similar in nature to those of the diffusive mechanism. Although at 10 K, the non-diffusive mechanism does not increase the abundance of either formaldehyde or methanol at early times, an increase is visible at times later than 10^5 yr. This increase is more visible in Fig. 4, where the abundance ratios of methanol and formaldehyde for Model 2 to Model 1 and Model 3 to Model 1

Downloaded from https://academic.oup.com/mnras/article/508/1/1526/6370606 by University of Virginia Law Library user on 06 July 2022

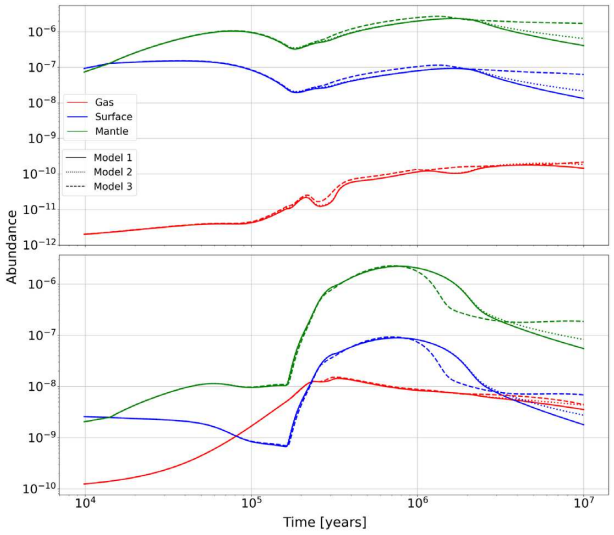

Figure 3. The abundances with respect to hydrogen nuclei of methanol (top panel) and formaldehyde (bottom panel) in Model 1, Model 2, and Model 3 at 20 K.

are plotted versus time. Essentially, all observed ratios greater than unity derive from Model 3.

The 10 K ratios in the top panel of Fig. 4 show increases up to a factor of 1.2 for methanol and 1.1 for formaldehyde. The methanol abundance ratios in the middle panel of Fig. 4 show an increase by over a factor of 3 at 15 K in the surface and mantle and little over a factor of 2 in the gas thereby doubling the amount of methanol in the gas and tripling in the ice after 10^5 yr. Formaldehyde shows a similar increase but to a lesser extent. The noticeable increase in difference between the ratios going from 10 to 15 K is accounted for by reduction in rate of the hydrogen addition reaction pathway in equation (1) as the hydrogen atoms on the grain surface begin to thermally desorb off the grains due to an increase in grain temperature. In comparison, the insertion mechanism into methane becomes more important due to its minimal temperature dependence. Model 3 to Model 1 comparisons at 20 K do not possess the large increases at 15 K because the rate of the insertion reactions decreases as the thermal desorption of methane begins to be more competitive at temperatures above 20 K. For both formaldehyde and methanol, any increases are similar in magnitude to those at 10 K except for the large surface and bulk gains after 10^6 yr caused by the insertion reaction into methane.

The results discussed above all result as a consequence of the $O(^1D)$ insertion into methane. However, it is crucial to understand that both of the insertion reactions of (4) and (5) are coupled with the hydrogen addition pathway of (1). Since reaction (5) produces formaldehyde, it feeds the supplied formaldehyde into the scheme of reaction pathway (1) which in turn can be fully saturated to form additional methanol either within the ices or in the gas phase via reactive desorption. Furthermore, any contribution to methanol and formaldehyde on the surface leads to increased desorption via hydrogen abstraction in which a hydrogen atom abstracts an additional hydrogen from a surface methanol or formaldehyde allowing another hydrogen atom to recombine with either CH_2OH/CH_3O or HCO which can desorb more species into the gas phase. Such addition and abstraction cycles provide more chances for desorption and have been suggested by Minissale et al. (2016).

4 ASTROPHYSICAL IMPLICATIONS

4.1 Additional insertion products

Though the increase in methanol and formaldehyde occurs by a small factor only, the insertion reactions show the potential to be significant for producing many other oxygen-bearing COMs in cold sources. An extension of the $O(^1D)$ insertion mechanism into methane was conducted by Bergner, Öberg & Rajappan (2019) with three hydrocarbons: ethane, ethylene, and acetylene. The authors found that ethanol and acetaldehyde were produced from ethane, acetaldehyde and ethylene oxide from ethylene, and ketene from acetylene. The insertion reactions with both ethane and acetylene were seen to proceed without barriers while the insertion into ethylene was seen to possess a small barrier of less than 100 K. Ethylene oxide production through insertion:

$$C_2H_4 + O(^1D) \rightarrow c\text{-}C_2H_4O, \quad (13)$$

could be a major contributor to the formation of this COM at low temperatures (<20 K) through the non-diffusive PDI mechanism as it would require no diffusion with a minimal barrier. However, at temperatures greater than 20 K, formation of ethylene oxide from the reaction between ethylene and the ground state of atomic oxygen, $O(^3P)$, can occur on grain surfaces (Ward & Price 2011) so that both cold and warm formation routes exist (Bergner et al. 2019). The warm formation route involving ground state oxygen has been previously modelled for the production of ethylene oxide and shown to be efficient during cloud collapse to form hot cores (Occhiogrosso et al. 2014).

In comparison to the insertion into methane, the insertion pathways into larger hydrocarbons could be more significant because the competitive production of molecules on a grain surface such as ethanol and acetaldehyde involves diffusion of large radicals; e.g.

$$CH_3 + CH_2OH \rightarrow CH_3CH_2OH, \quad (14)$$

$$CH_3 + HCO \rightarrow CH_3HCO, \quad (15)$$

and is therefore more inhibited by diffusion barriers at low temperatures.

Overall, the reactivity of $O(^1D)$ is not limited to only the experimentally studied hydrocarbons. Because non-diffusive chemistry requires that $O(^1D)$ react with a nearest neighbour surface species, reaction will be most favourable with highly abundant ice components such as CO and CO_2. Granular reactions with both carbon monoxide and carbon dioxide could lead to the formation of CO_2 and CO_3, respectively, which have been observed product channels in gas phase insertions (Raper & DeMore 1964; Young & Ung 1966). Difficult to form at low temperatures from low diffusivity of reactants, CO_2 has been known to form on grain surfaces from the HOCO intermediate produced from the reaction between CO and OH, which can be initiated by O and H atoms diffusing rapidly to form OH atop a CO molecule (Jin & Garrod 2020). The insertion reaction by $O(^1D)$ could further add to the carbon dioxide abundance especially in slightly warmer environments where the diffusion of hydrogen becomes inhibited by thermal desorption. CO_3 provides a starting point to form carbonic acid (H_2CO_3) upon two hydrogen additions. Though not detected in any interstellar sources, this carboxylic acid could play a role in interstellar chemistry. The non-detection may be due to its nature of undergoing a proton transfer with ice species such as NH_3 to form an acid base pair in the ice (Oba et al. 2010).

Two additional molecules that could be potential products of oxygen insertion reactions are hydroxylamine (NH_2OH) and methane-

Downloaded from https://academic.oup.com/mnras/article/508/1/1526/6370606 by University of Virginia Law Library user on 06 July 2022

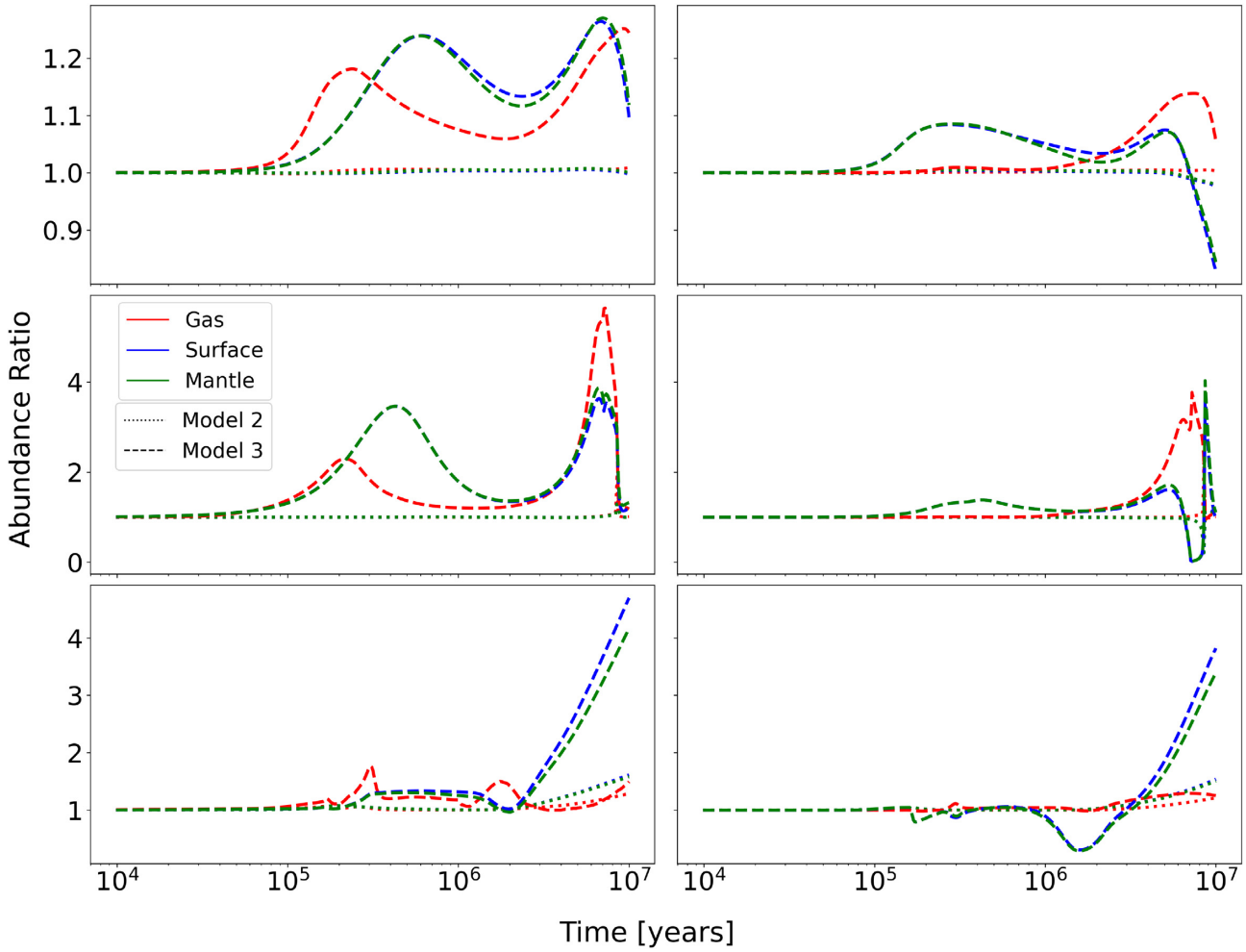

Figure 4. The abundance ratios for Model 2 to Model 1 (dotted lines) and Model 3 to Model 1 (dashed lines) of methanol (left-hand panel) and formaldehyde (right-hand panel). Temperatures shown are 10 (top panel), 15 (middle panel), and 20 K (bottom panel).

diol ($HOCH_2OH$). While hydroxylamine can be formed from the radical recombination of NH_2 and OH, a more efficient low-temperature mechanism is the hydrogenation of NO on the surface of ices (Congiu et al. 2012). The non-diffusive $O(^1D)$ insertion into solid phase ammonia provides a direct pathway towards hydroxylamine which could be competitive with the hydrogenation route. Due to the large abundances of methanol on grains, an insertion by $O(^1D)$ into methanol can result in the formation of methanediol, which is a theoretically predicted reaction pathway (Hays & Widicus Weaver 2013).

4.2 Other metastable species

Insertion reactions are not only unique to oxygen atoms; other metastable atoms or molecules can possess similar reactivity. One such species is the carbon atom, with a related electronic structure to oxygen leading to both a ground ^3P state and an excited metastable ^1D state. Experimental work has been conducted on the reactivity of $C(^1D)$ with H_2 (Hickson et al. 2015), CO_2 (Nuñez-Reyes & Hickson 2018), and CH_4 (Nuñez-Reyes & Hickson 2017) as examples. These works involve gas phase reactivity, which typically lead to dissociation channels, as was seen in oxygen insertions. However, any grain surface reactions will prefer the insertion process by forming closed-shell products due to the excess reaction energy being dissipated efficiently.

5 CONCLUSIONS

This work investigates the contribution of insertion reactions between $O(^1D)$ and methane to the formation of methanol and formaldehyde on interstellar ices in cold cores and slightly warmer pre-stellar core conditions at temperatures from 10 K through 20 K. The standard version of `Nautilus-1.1` (Ruaud et al. 2016) was expanded to include the insertion reaction into methane experimentally observed by Bergner et al. (2017). The reaction was modelled utilizing both the standard diffusion mechanism and the PDI mechanism first formulated by Garrod (2019) where the photoproduced $O(^1D)$ reacts immediately with nearby neighbours. The diffusive mechanism was seen to be inefficient in the production of methanol and formaldehyde in comparison to the multistep hydrogen addition of CO, as shown in equation (1). The non-diffusive mechanism, however, shows a more rapid production of methanol and formaldehyde, where the effect is seen to increase from 10 to 15 K but with less of a contribution at 20 K. This mechanism at its peak shows a methanol increase of over a factor of 2 in all phases at 15 K confirming a competitiveness with the CO hydrogenation mechanism. Future models could prove that these granular insertion reactions are efficient at creating larger COMs such as observed by Bergner et al. (2019), who studied the formation of ethanol, acetaldehyde, ethylene oxide, and ketene upon insertion of $O(^1D)$ into C_2 hydrocarbons. Further work is still needed

Downloaded from https://academic.oup.com/mnras/article/508/1/1526/6370606 by University of Virginia Law Library user on 06 July 2022

to elucidate all possible reaction paths involving photoproduced metastable oxygen or other metastable species to fully ascertain the contributions of insertion reactions under interstellar conditions.

ACKNOWLEDGEMENTS

E. H. thanks the National Science Foundation (US) for support of his research programme in astrochemistry through grant AST 19-06489. We would like to thank V. Wakelam for the usage of the `Nautilus-1.1` program.

DATA AVAILABILITY

These data underlying this article are available in the article as well as cited online kinetic data repositories, especially Kinetic Database for Astrochemistry (KIDA) via its URL https://astrophy.u-bordeaux.fr.

REFERENCES

Agúndez M., Marcelino N., Tercero B., Cabezas C., de Vicente P., Cernicharo J., 2021, A&A, 649, 6
Atkinson R. et al., 2007, Atmos. Chem. Phys., 7, 981
Bergner J. B., Öberg K. I., Rajappan M., 2017, ApJ, 845, 29
Bergner J. B., Öberg K. I., Rajappan M., 2019, ApJ, 874, 115
Bieler A. et al., 2015, Nature, 526, 678
Blake G. A., Sutton E. C., Masson C. R., Phillips T. G., 1987, ApJ, 315, 621
Chichinin A. I., 2000, Chem. Phys. Lett., 316, 425
Congiu E. et al., 2012, ApJ, 750, 4
Davidson J. A., Schiff H. I., Streit G. E., McAfee J. R., Schmeltekopf A. L., Howard C. J., 1977, J. Chem. Phys., 67, 5021
DeMore W. B., Raper O. F., 1967, J. Chem. Phys., 46, 2500
Draine B. T., 1978, ApJS, 36, 595
Dunlea E. J., Ravishankara A. R., 2004a, Phys. Chem. Chem. Phys., 6, 2152
Dunlea E. J., Ravishankara A. R., 2004b, Phys. Chem. Chem. Phys., 6, 3333
Fuchs G. W., Cuppen H. M., Ioppolo S., Romanzin C., Bisschop S. E., Andersson S., van Dishoeck E. F., Linnartz H., 2009, A&A, 505, 629
Garrod R. T., 2019, ApJ, 884, 69
Garrod R. T., Wakelam V., Herbst E., 2007, A&A, 467, 1103
Garrod R. T., Widicus Weaver S. L., Herbst E., 2008, ApJ, 682, 283
Gibb E. L., Whittet D. C. B., Boogert A. C. A., Tielens A. G. G. M., 2004, ApJS, 151, 35
Graedel T. E., Langer W. D., Frerking A. D., 1982, ApJS, 48, 321
Hasegawa T. I., Herbst E., Leung C. M., 1992, ApJS, 82, 167
Hays B. M., Widicus Weaver S. L., 2013, J. Phys. Chem., 117, 7142
Heays A. N., Bosman A. D., van Dishoeck E. F., 2017, A&A, 602, A105
Heidner R. F., Husain D., 1973, Nat. Phys. Sci., 241, 10
Hickson K. M., Loison J.-C., Guo H., Suleimanov Y. V., 2015, J. Phys. Chem., 6, 4194
Hiraoka K., Miyagoshi T., Takayama T., Yamamoto K., Kihara Y., 1998, ApJ, 498, 710
Jenkins E. B., 2009, ApJ, 700, 1299
Jin M., Garrod R. T., 2020, ApJS, 249, 26
Lam L., Hastie D. R., Ridley B. A., Schiff H. I., 1981, J. Photochem., 15, 119
Lee K. L. K. et al., 2021, ApJ, 910, 7
McGuire B. A., Berkhardt A. M., Kalenskii S., Shingledecker C. N., Remijan A. J., Herbst E., McCarthy M. C., 2018, Science, 359, 202
Minissale M., Moudens A., Baouche S., Chaabouni H., Dulieu F., 2016, MNRAS, 458, 2953
Mohammed H. H., 1990, J. Chem. Phys., 93, 412
Ndengué S., Madronich S., Gatti F., Meyer H.-D., Motapon O., Jost R., 2014, J. Geophys. Res., 119, 4286
Neufeld D. A., Wolfire M. G., Schilke P., 2005, ApJ, 628, 260
Nuñez-Reyes D., Hickson K. M., 2017, J. Phys. Chem., 121, 3851
Nuñez-Reyes D., Hickson K. M., 2018, J. Phys. Chem., 122, 4002
Oba Y., Watanabe N., Kouchi A., Hama T., Pirronello V., 2010, ApJ, 722, 1598
Öberg K. I., Bottinelli S., Jørgensen J. K., van Dishoeck E. F., 2010, ApJ, 716, 825
Öberg K. I., Boogert A. C. A., Pontoppidan K. M., van den Broek S., van Dishoeck E. F., Bottinelli S., Blake G. A., Evans N. J. II, 2011, ApJ, 740, 16
Occhiogrosso A., Vasyunin A., Herbst E., Viti S., Ward M. D., Price S. D., Brown W. A., 2014, A&A, 564, 9
Prasad S. S., Tarafdar S. P., 1983, ApJ, 267, 603
Qasim D., Fedoseev G., Chuang K. J., He J., Ioppolo S., van Dishoeck E. F., Linnartz H., 2020, Nat. Astron., 4, 781
Raper O. F., DeMore W. B., 1964, J. Chem. Phys., 40, 1053
Ruaud M., Wakelam V., Hersant F., 2016, MNRAS, 459, 3756
Schmidt J. A., Johnson M. S., Schinke R., 2013, Proc. Natl. Acad. Sci., 110, 17691
Shingledecker C. N., Tennis J., Le Gal R., Herbst E., 2018, ApJ, 861, 20
Slanger T. G., Black G., 1982, J. Chem. Phys., 77, 2432
Takahashi K., Wada R., Matsumi Y., Kawasaki M., 1996, J. Chem. Phys., 100, 10145
Talukdar R. K., Ravishankara A. R., 1996, Chem. Phys. Lett., 253, 177
Taquet V., Furuya K., Walsh C., van Dishoeck E. F., 2016, MNRAS, 462, S99
Wakelam V., Herbst E., 2008, ApJ, 680, 371
Wakelam V. et al., 2012, ApJS, 199, 21
Wakelam V., Loison J. C., Mereau R., Ruaud M., 2017, Mol. Astrophys., 6, 22
Ward M. D., Price S. D., 2011, ApJ, 741, 121
Watanabe N., Kouchi A., 2002, ApJ, 571, L173
Wiese W. L., Smith M. W., Miles B. M., 1966, Atomic Transition Probabilities Hydrogen Through Neon, National Standard Reference Data Series. National Bureau of Standards, Washington, D.C.
Young R. A., Ung A. Y.-M., 1966, J. Chem. Phys., 44, 3038

This paper has been typeset from a TEX/LATEX file prepared by the author.

Downloaded from https://academic.oup.com/mnras/article/508/1/1526/6370606 by University of Virginia Law Library user on 06 July 2022